Photodissociation Dynamics of *tert*-Butyl Nitrite on Ag(111): Characterization of Translationally and Internally Excited NO Fragments†

W. Zhao, C. Kim, and J. M. White*

Department of Chemistry & Biochemistry, Center for Materials Chemistry, University of Texas at Austin, Austin, Texas 78712-1167

S. K. Kim

Department of Chemistry, Sungkyunkwan University, Suwon, 440-746, Korea

Received: August 28, 2000; In Final Form: November 21, 2000

The translational, vibrational, and rotational characteristics of nitric oxide, NO, ejected by 351 nm photodissociation of *tert*-butyl nitrite, $(CH_3)_3CONO$, adsorbed on Ag(111) have been investigated using resonance-enhanced multiphoton ionization time-of-flight (REMPI-TOF) and interpreted using a direct excitation and collisional relaxation model. There are three translational energy components denoted as collisionless, intermediate, and thermalized. The collisionless component has characteristics matching those found for gas phase monomer photolysis. The thermalized component has characteristics expected for NO accommodated to the substrate temperature, while the more complex intermediate component is qualitatively describable in terms of collisions of nascent energetic NO with surrounding species as it exits into the gas phase. There are strong $v'' = 1$ and 2 but negligible $v'' = 0$ contributions to the collisionless component. The collisionless component is also characterized by high rotational excitation; Gaussian rotational distributions with $J_{max} = 24.5 \pm 1$ for $v'' = 1$ and 29.5 ± 1 for $v'' = 2$ provide reasonable fits. The translationally thermalized component is dominated by the $v'' = 0$ vibrational state and by a Boltzmann rotational distribution ($T_{rot} = 124 \pm 30$ K); i.e., all three modes of motion are thermalized. The vibrational and rotational characteristics of the intermediate translational component are more complex and will require simulation and angle-resolved REMPI for fuller elucidation.

1. Introduction

While research over the last two decades has probed the dynamics of surface processes,[1−4] it remains challenging to determine how energy released during a surface reaction is distributed among the products. A photon-induced surface reaction that leads directly to gas-phase products can be investigated by using state specific techniques to determine the vibrational and rotational states, velocity distributions, and rotational alignment of these products. The dynamics are then inferred by comparing the product state distributions with the gas phase, a simple dynamical model, or molecular dynamics simulations. Ongoing interest is driven by fundamental issues concerning the mechanisms of molecular dissociation and energy transfer from the radiation field, as well as by technical applications, such as photochemical etching and deposition.[5,6]

The gas-phase photodissociation of alkyl nitrite molecules has been studied extensively; UV radiation dissociates the alkyl nitrite molecule into an alkoxy fragment and NO.[7−24] Above 200 nm, the gas-phase UV absorption spectrum of the alkyl nitrites displays two excitation bands, S_1 and S_2. Between 219 and 300 nm, unstructured absorption occurs to S_2, the internal NO bond dissociates, and the photodissociation produces rotationally hot but vibrationally cool NO molecules. Above 300 nm, S_1 is accessed, and the molecule dissociates, but the absorption spectrum exhibits a well-resolved progression associated with the stretching of the external N═O bond. The vibrational distribution of the nascent NO peaks at one quantum below that reached in exciting the nitrite.

As an example, the photolysis of gas phase *tert*-butyl nitrite (TBN) has been studied extensively. Rosenwaks et al.[8,11−13] examined *monomer* TBN photodissociation and found that the scalar properties of the NO fragment are very different for the S_2 and S_1 excited states. Whereas S_1 excitation produces wavelength dependent vibrationally excited NO, S_2 produces vibrationally cold NO. S_1 excitation of TBN gas phase *clusters* produces a bimodal rotational distribution,[22] the high-*J* portion having kinetic energy comparable to that for monomer dissociation, while the low-*J* portion has much lower kinetic energy. The latter portion is discussed in terms of collisions of nascent NO within the clusters.

Simpson et al.[25−27] measured state-resolved translational and rotational energy distributions of NO from 351 nm photolysis of *tert*-butyl nitrite adsorbed on MgF_2. The translational distribution was broad with a single maximum, while the rotational distribution was bimodal and nicely characterized as the sum of Boltzmann and Gaussian components. The dielectric surface of MgF_2 neither quenched the excited S_1 state nor thermalized the NO photoproduct.

Jenniskens and co-workers[28−31] examined the 355 and 266 nm photodissociation of TBN on Ag(111). Coverage-dependent bimodal translational energy distributions were observed and fit with the sum of hyperthermal and thermal Boltzmann distributions. The total photodissociation cross section was similar to that found for gas-phase photodissociation, and the

† Part of the special issue "Aron Kuppermann Festschrift".

10.1021/jp003101s CCC: $20.00
Published on Web 01/25/2001

characteristic energy of the hyperthermal distribution increased with photon energy. The results support a direct excitation mechanism in which the photodissociation is initiated when *tert*-butyl nitrite absorbs a photon; there was no evidence for substrate-mediated excitation of TBN.

Earlier, Pressley et al.[32] investigated thermal, electron, and photon activation of methyl nitrite, and more recently, enhancing the time resolution of Jenniskens' work,[28−31] Fieberg et al.[33,34] measured angle-resolved TOF distributions of NO from TBN and methyl nitrite photolysis and found obvious trimodal NO velocity distributions. The three components were assigned to NO undergoing no collisions, a few collisions, and thermalizing collisions. As for TBN, there was no evidence for substrate-mediated excitation.

Kim et al.[35] investigated the *internal* state-resolved dynamics of NO produced by 248 nm photodissociation of TBN using REMPI-TOF. For high rotational states ($J > 30$) the translational energy distribution is dominated by fast, highly nonthermal NO desorption, designated collisionless. For low rotational states ($J < 20$) there are two readily distinguished peaks in the translational energy distribution, designated as intermediate and thermalized components. As for earlier work, the results conform to direct photodissociation with no measurable contributions from substrate-mediated excitation. Zhao et al.[36] measured the rotational and electronic state distributions of the NO photofragments produced at 248 nm. The fastest NO is characterized by a quite narrow nonthermal Gaussian distribution of high-J states, peaking at $J = 54.5 \pm 1$, while the slowest NO is characterized by a Boltzmann distribution of low-J states with a temperature close to that of the substrate (∼100 K). The spin−orbit population ratio, $n(F_1)/n(F_2)$, of NO is near unity for collisionless trajectories and increases to 3.9 for thermalized trajectories.

In this paper we focus on excitation into S_2 and report state-resolved (translation, vibration and rotation) NO data for excitation at 351 nm, which in the gas phase selectively excites TBN with 3 quanta in the RON═O stretching mode.

2. Experimental Section

The ultrahigh vacuum (UHV) chamber and laser system is described in more detail elsewhere.[33−36] Briefly, the experiments were done in a two-level UHV chamber, which operates at a base pressure of $< 2 \times 10^{-10}$ Torr. An ion gun, reverse-view low-energy electron diffraction (LEED) apparatus, and Auger electron spectrometer comprise the upper level, where the substrate is cleaned and analyzed. Dosing, photoinduced reactions and REMPI-TOF state-resolved measurements are pursued on the lower level. A rotatable quadrupole mass spectrometer (QMS) for angle-resolved TOF experiments is located on the same level.

Standard substrate cleaning procedures were followed.[33,34] With a newly designed sample mount, the Ag(111) substrate temperature reached 78 K in less than 15 min by contact with a liquid nitrogen reservoir. Heating was accomplished resistively and was limited to 850 K in order to avoid silver evaporation. The crystal preparation process was described previously.[33] TBN was freeze−pump−thawed several times to reduce the impurity level of butanol to less than 3%. TBN was dosed through a leak valve connected to a 3 mm ID tube that was directed at and terminated 1 cm from the front face of the substrate. The relative *tert*-butyl nitrite coverage was calibrated by TPD measurements, assigning separable peaks to monolayer and multilayers.

Adsorbed TBN was photolyzed using an excimer laser (Lambda Physik COMPex 102M), operating at 351 nm. Figure 1 is a schematic of the optical system. To reduce the laser output below 0.3 mJ/cm^2, the output pulses were attenuated with a metal mesh and several neutral density filters. No more than 15% of the adsorbate was photodissociated in a typical REMPI-TOF experiment (∼2000 pulses).

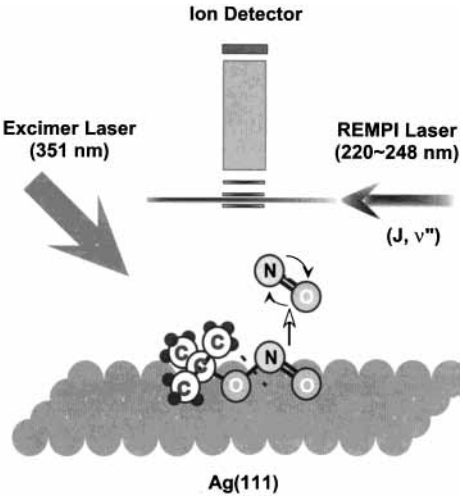

Figure 1. Schematic of the REMPI-TOF experiment.

The desorbing NO was characterized using a two-photon (1 + 1) REMPI-TOF scheme. The fundamental wavelength of a Nd:YAG laser (Continuum PL7010) was tripled to 355 nm to pump the dye laser (Lambda Physik Scanmate II). Coumarin 2 and 102 dye solutions were used for examining NO vibrational states $v'' = 0$ and $v'' = 1$ or 2, respectively. The output of the dye laser was doubled using a BBO-B crystal (Inrad Autotracker II), and the dye laser fundamental output was rejected using a harmonic separator (Inrad 752−104). The REMPI laser beam (∼1 mJ/pulse, 12 ns) traveled parallel to the substrate surface and was focused by a cylindrical lens at a distance of 35 ± 2 mm from the plane of the surface. The NO^+ ions were formed by REMPI at selected delay times after the excimer laser pulse and were monitored using a Wiley−McLaren type time-of-flight device that contained a microchannel plate (MCP) detector. The ion signal was gated, read into a boxcar integrator, and output to a computer interface. The REMPI laser intensity was monitored by a photodiode, and its signal was used to normalize the measured NO^+ signals. A digital delay/pulse generator controlled the time delay between the photolysis and probe lasers.

In all the work reported here, the NO REMPI-TOF spectra were collected with the detector located along the surface normal, as in Figure 1. The resulting density domain data were least-squares fit to n ($n = 2$ or 3 in these experiments) modified Maxwell−Boltzmann (MB) distributions:

$$I(t) = \frac{1}{t^4}\sum_{i=1}^{n} a_i \exp\left[-b_i\left(\frac{d}{t} - v_{o,i}\right)^2\right] + BG(t) \qquad (1)$$

Here $I(t)$ is the total counts summed from n distributions, t is the flight time, a_i is the amplitude of the ith component, b_i is a fitting parameter from which an effective temperature T_i can be calculated from $b_i = m/2k_BT_i$, d is the flight distance from the sample to the REMPI laser, and $v_{o,i}$ is the common velocity of the ith component. If the ith distribution is close to thermal equilibrium, $v_{o,i}$ is 0, and T_i is the temperature of the distribution, which is equivalent to average kinetic energy $\langle E_i \rangle$ divided by $2k_B$. Description of nonequilibrium distributions that are narrower than Maxwell−Boltzmann (MB) requires $v_{o,i}$ larger than

TABLE 1: Velocities (m s^{-1}) Calculated for Fits to TOF Spectra of Figure 2

	NO ($J = 28.5$)			NO ($J = 7.5$)		
	(a) collisionless	(c) intermediate	(b) thermalized	(a) collisionless	(c) intermediate	(b) thermalized
$v'' = 2$	1556	1250	none	1556	1296	none
$v'' = 1$	1576	1296	none	1556	1207	368
$v'' = 0$	none	1250	none	none	1167	364

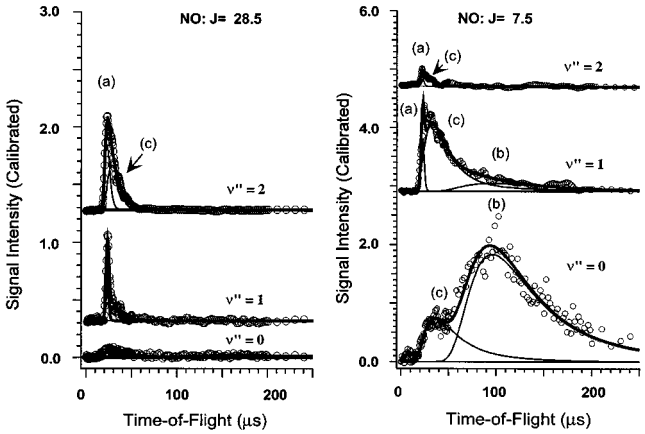

Figure 2. TOF spectra of NO produced by 351 nm photodissociation of 5.0 ML *tert*-butyl nitrite on Ag(111) at the indicated combinations of J and v''. The thin solid lines are modified Maxwell−Boltzmann fits, and the dashed lines are the summation of the thin solid lines. Three components are labeled on various curves: (a) collisionless; (b) thermalized; (c) intermediate. Note that only $J = 7.5$ and $v'' = 2$ require three components.

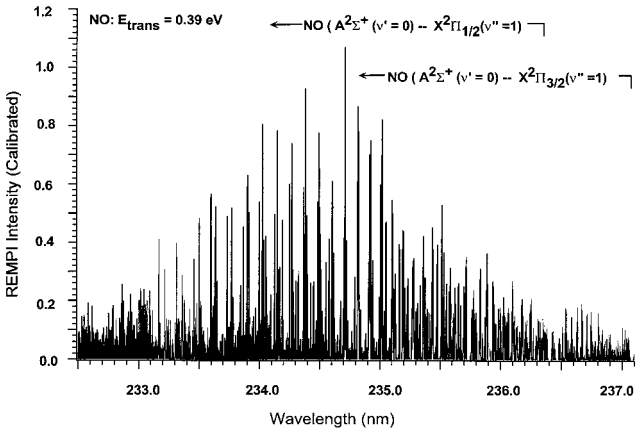

Figure 3. Experimental (1 + 1) REMPI spectra of the NO A$^2\Sigma^+$ ($v' = 0$) ← NO X$^2\Pi$ ($v'' = 1$), NO, $E_{trans} = 0.39$ eV, desorbed from 40 ML *tert*-butyl nitrite photolysis on Ag(111) surface. The signal intensity is adjusted for laser fluctuation and coverage decay (see text).

0. As noted recently,[37] care must be exercised when assigning an effective temperature to such distributions. Here, we report the velocities extracted from the fits. The factor $BG(t)$ is included to account for the time required to evacuate the desorbing NO.

$$BG(t) = a(1 - e^{-b(t-to)}) \quad t \geq t_o \qquad (2)$$

$$= 0 \quad t < t_o$$

where a is a proportionality constant, b is a time constant characteristic of the pumping system, and t_o is the onset time.

3. Results

3.1. Translational Velocity Distributions. Figure 2 shows time-of-flight (TOF) spectra of ejected NO photofragments for $v'' = 0$, 1, and 2 at $J = 7.5$ and 28.5 during 351 nm laser photodissociation of 5.0 ML TBN on Ag(111). With one exception requiring three components, each spectrum was fit satisfactorily to eq 1 by two components (thin solid lines in Figure 2). The dashed line is the sum of the thin solid lines. The velocities that fit the spectra are summarized in Table 1 and fall into three regimes labeled a−c in Figure 2. Component b is slowest (368 ± 10 m s^{-1}) and appears only for the $J = 7.5$ and $v'' = 0$ and 1 spectra. Component a is fastest (1560 ± 40 m s^{-1}) and is the same for $v'' = 1$ and 2 and for $J = 28.5$ and 7.5. Interestingly, this component makes no detectable contribution to the $v'' = 0$ spectra. The peaks in component c vary with vibrational state and have intermediate velocities ranging from 1167 to 1296 m s^{-1}. These three components are attributed to collisionless ejection (a), release after becoming fully thermalized (b), and ejection after one or a few collisions (c). We conclude that, as for 248 nm photolysis,[35,36] there is correlation among translational, vibrational, and rotational energies. For example, NO arriving at the detector with little rotational and vibrational energy is also moving slowly, component b, whereas rapidly moving NO, component a, includes negligible amounts of NO in $v'' = 0$.

3.2. Internal State Distributions. The two-photon excitation spectra of the NO A$^2\Sigma^+$ ($v' = 0$) ← NO X$^2\Pi$ ($v'' = 0$, 1, 2) transitions are known from the literature,[38−44] and the analysis procedure used to extract rotational and vibrational state distributions was similar to that described previously.[36] Briefly, experimental spectra were compared with the spectra calculated using the known spectroscopic constants[40] by convoluting computed spectral lines with an experimental bandwidth. To assign the J levels populated in the NO X$^2\Pi$ v'' fragments, the relative spectral positions of individual rotational transitions up to $J = 75.5$ have been calculated using literature values.[40] Since the REMPI laser wavelength was not independently calibrated, the calculated spectra were shifted slightly to match with the experimental spectra.

The NO rotational state distribution at a particular NO translational energy was obtained by scanning the REMPI laser wavelength for a selected delay time. Experimentally, this is formidable because a wide range of wavelengths must be scanned, during which the photochemistry alters the surface composition. Given these difficulties, we chose to dose as much as 40 ML TBN for every 0.5 nm wavelength scan and kept an overlap of 0.1 nm between two adjacent scans. The signal intensities in the overlap region were used to normalize the spectra to each other. The REMPI intensity was also normalized for laser fluctuations.

Figure 3 shows the REMPI spectrum of NO A$^2\Sigma^+$ ($v' = 0$) ← NO X$^2\Pi$ ($v'' = 1$). The time delay between photolysis and probe lasers was set at 22 μs to monitor the fastest NO component; i.e., $E_{trans} = 0.39$ eV. The same experiment was done for the transition NO A$^2\Sigma^+$ ($v' = 0$) ← NO X$^2\Pi$ ($v'' = 2$). The R21 branch of NO two-photon excitation was chosen to represent the rotational distributions. Taking into account two-photon Hönl−London intensity factors, Figure 4a summarizes the NO rotational state distributions for these two cases. Fitting with Gaussian distributions yielded $J_{max} = 24.5 \pm 1$ at $v'' = 1$ and $J_{max} = 29.5 \pm 1$ at $v'' = 2$. As indicated in Figure 2 for J

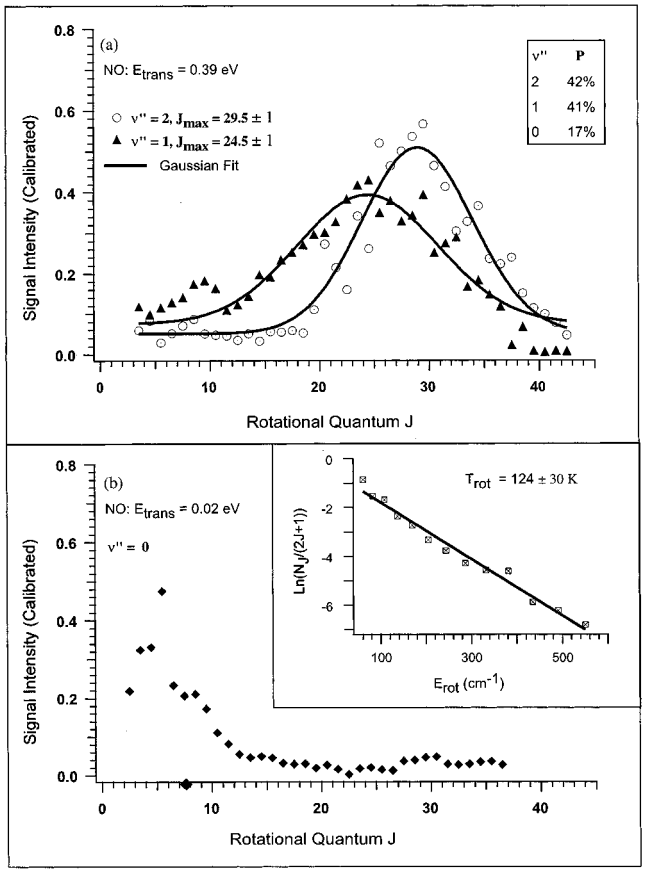

Figure 4. (a) Rotational state distributions of the collisionless NO (E_{trans} = 0.39 eV) produced in vibrational levels $v'' = 1$ and 2. The solid lines are Gaussian fits. (b) The rotational state distribution of the thermalized NO produced in the vibrational state $v'' = 0$. The insert is a Boltzmann fit, and $T_{rot} = 124 \pm 30$ K.

= 28.5 and 7.5, NO ejected with $v'' = 0$ exhibits only components b and c, i.e., a negligible signal at 22 μs. This holds for all J states. It is noteworthy that for $v'' = 1$, the fit is satisfactory except for low J (<10.5), where the relative intensity is higher than expected for a Gaussian fit. Evidently, energy transfer occurs during dissociation to eject collisionless and vibrationally excited low-J rotational states.

The rotational distribution measured for region b of Figure 2 (time delay of 100 μs) for NO produced in $v'' = 0$ is shown in Figure 4b. The insert is a fit to a presumed thermal distribution and the slope yields a characteristic T_{rot} of 124 ± 30 K, reasonably close to the surface temperature of 80 K.

Turning to vibrations, assessment of vibrational populations requires summing over all excited rotational levels in each vibrational state. The REMPI intensity is related to the population of the corresponding electronic ground-state rovibronic state $N(J,v'')$. To proceed, we first obtained the rotational distribution for each vibrational state measured at the peak of the collisionless component a for $v'' = 1$ and 2 and at the peak of the thermalized component b for $v'' = 0$. Ratios of the integrated rotational distribution for each vibrational state were then divided by the corresponding Franck−Condon factors to yield relative vibrational populations. This method reduces errors caused by scatter in the intensities of different lines. Since $v'' = 3$ may contribute but was not accessible in our experiment, we report relative populations. For component a at 22 μs, this procedure yields 0% in $v'' = 0$, 41% in $v'' = 1$, and 42% in $v'' = 2$. For component b at 100 μs, there is >95% in $v'' = 0$, <5% in $v'' = 1$, and 0% in $v'' = 2$. Comparison with monomer gas-phase photolysis is discussed below.

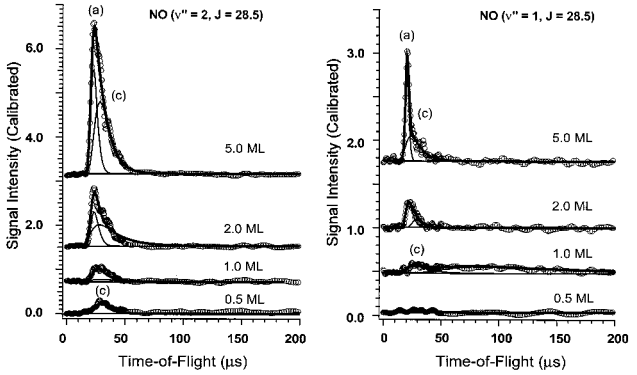

Figure 5. REMPI measurements at $J = 28.5$ and $v'' = 1$ and 2 for submonolayer to multilayer coverages of TBN on Ag(111). The thin solid lines are modified Maxwell−Boltzmann fits, and the heavy solid lines are the summations of the thin solid lines. Components are labeled as (a) collisionless and (c) intermediate.

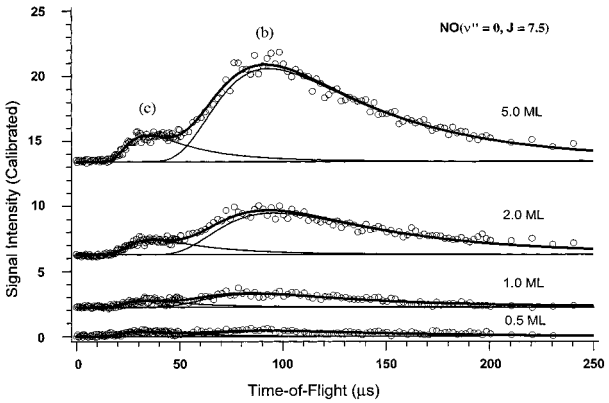

Figure 6. Coverage-dependent REMPI measurements at $J = 7.5$ and $v'' = 0$ for submonolayer to multilayer coverages of TBN on Ag(111). The thin solid lines are modified Maxwell−Boltzmann fits, and the heavy solid lines are the summations of the thin solid lines. Components are labeled as (b) thermalized and (c) intermediate.

3.3. Coverage Dependence. Figures 5 and 6 show the recorded state-resolved REMPI-TOF spectra for the indicated combinations of J and v'' for selected coverages between 0.5 and 5 ML. The thin solid lines are modified Maxwell−Boltzmann fits, and the heavy solid lines are the summation of the two thin lines. The fastest moving, high-J, and vibrationally excited NO component, labeled a in Figure 5, is not detectable at or below 1 ML. Between 1 and 5 ML it grows monotonically. It is also noteworthy that at the lowest coverage, 0.5 ML, there is a detectable intermediate component for $v'' = 2$ but not for $v'' = 1$ or 0, labeled c in Figures 5 and 6. Not surprisingly, based in Figure 4, there is no detectable component b in the $J = 28.5$ spectra, regardless of the coverage, i.e., no signal at 100 μs.

For thick multilayer coverages (Figure 4) and $J = 7.5$, there is a large signal at 100 μs for $v'' = 0$ and some signal at 22 μs for $v'' = 1$ but not $v'' = 2$. Time-of flight spectra for selected coverages, $v'' = 0$ and $J = 7.5$ are shown in Figure 6. Components b and c both increase monotonically with coverage. Component b, fully rotationally, vibrationally, and translationally thermalized according to Figure 4, dominates these spectra at all coverages. Component c has a complicated dependence on coverage, and the position of its maximum depends on the rotational state selected.

4. Discussion

Gas-Phase Monomer Photochemistry. The gas-phase photodissociation of TBN[45] can be described with following reaction sequence

$$(CH_3)_3CONO\ (S_0) + h\nu \rightarrow (CH_3)_3CONO^*\ (S_1 \text{ or } S_2)$$

$$(CH_3)_3CONO^*\ (S_1 \text{ or } S_2) \rightarrow (CH_3)_3CO\ (A \text{ or } X) + NO\ (X^2\Pi)$$

and occurs on different potential energy surfaces (PES), which can be characterized by two coordinates R_{O-N} and $R_{N=O}$. The gas-phase S_2 PES is repulsive and monotonically decreasing along the R_{O-N} coordinate; i.e., there is no barrier hindering immediate fragmentation once the molecule is photoexcited in the wavelength range between 216 and 300 nm. In this direct photodissociation, the coupling between the R_{O-N} and $R_{N=O}$ coordinates is weak, and the exiting NO is ejected with little vibrational excitation.

In contrast, the gas-phase S_1 PES has a shallow minimum near the Franck−Condon transition region and the coupling between R_{O-N} and $R_{N=O}$ is much stronger in the sense that extension of R_{O-N}, the bond that breaks, is inextricably connected to vibrational excitation of the $R_{N=O}$ stretch. Upon photon absorption, the immediate path of steepest descent involves motion along the $R_{N=O}$ coordinate. Calculations predict that S_1 excited nitrites live for 5−10 vibrational periods of $R_{N=O}$ before R_{O-N} breaks. Thus, the photodissociation of TBN through the S_1 state is characterized as a vibrational predissociation process.

When TBN is condensed or adsorbed, other coordinates (degrees of freedom) are introduced. These account for the ground- and excited-state interactions between TBN and both the substrate and other TBN interactions that influence the photodissociation and subsequent dynamics, e.g., the translational and internal state distributions of ejected NO.

Translational Velocity Distributions. As in our previous 248 nm photolysis study,[35,36] the 351 nm photodissociation of TBN on Ag(111) exhibits trimodal translational distributions (Figure 2), with collisionless (a), intermediate (b), and thermalized (c) components. Bimodal distributions have been reported for photolysis of molecular clusters of TBN[22] and for TBN on MgF_2.[26] For the latter, hyperthermal NO was noted, with energies up to 0.62 eV.

The characteristic translational energy of the collisionless NO depends on the photon energy; the peak appears at 22 μs time delay (0.39 eV) for 351 nm, in contrast to NO at 15 μs (0.85 eV) for 248 nm photolysis. The characteristic energy (0.39 eV = 3146 cm^{-1}) is very close to 2950 cm^{-1} found in the gas-phase photodissociation of TBN[13] and is taken to mean that the NO is produced from the topmost layer of the TBN-covered surface and is ejected without colliding with either neighbors or the substrate.

The thermalized NO, as expected for accommodation with the surface temperature, has the same kinetic energy for both wavelengths, peaking near 100 μs (368 m s^{-1}). Figures 5 and 6 show that the intensities, but not the kinetic energies, of the collisionless and thermalized NO components are coverage-dependent.

The intermediate component is widely distributed and is of central interest in simulation studies now underway in our laboratory. The variations among reports are, we believe, related to contributions of this component that we have been able to resolve with better time and state resolution.

Another striking feature of our results is the correlation among translational, rotational and vibrational energies. Figure 2 reveals that high translational energy is correlated with high rovibronic energy, just as in gas-phase photolysis. Lower translational energy is correlated to lower rotational and vibrational energy, because interactions between energetic NO photoproducts and the surface or neighboring species tend to thermalize all these components. Recently, the photolysis of H_2S adsorbed on LiF(001) was studied by hydrogen Rydberg-atom TOF spectroscopy in the Polanyi group.[46] As here, the H-atom translational energy distribution showed three main features, and a similar relaxation model was proposed.

Rotational State Distribution. The bimodal rotational state distribution of NO has been discussed in alkyl nitrite cluster photodissociation;[22] our current results follow the trend (Figure 4). The rotational state distributions of the collisionless NO (E_{trans} = 0.39 eV), nicely fit with Gaussian distributions, are centered at $J_{max} = 29.5 \pm 1$ for $v'' = 2$ and $J_{max} = 24.5 \pm 1$ for $v'' = 1$. A Boltzmann thermal distribution with $T_{rot} = 124 \pm 30$ K fits the rotational states at $v'' = 0$.

The rotational state distribution of the photoproduct NO is a very sensitive probe of the NO escape mechanism since it is very easily distorted by collisions with the substrate and neighboring species. For the collisionless translational component produced in $v'' = 2$, $J_{max} = 29.5 \pm 1$ is in agreement with gas-phase monomer photolysis ($J_{max} = 31.5$).[13] TBN photolysis on MgF_2 showed similar behavior.[26] Whereas we find measurably smaller J_{max} for NO with $v'' = 1$ than $v'' = 2$, the reverse holds for gas-phase photodissociation.

As in previous work, we attribute the thermalized component to NO molecules, which are trapped momentarily at the surface after the internal O−N bond breaks.

Vibrational State Distribution. For gas phase monomer photolysis at 351 nm, there is barely detectable population at $v'' = 0$ (about 1%).[13] The relatively high population of $v'' = 0$ we observe is consistent with the work of Kades et al.[22] on TBN clusters. We take this as reflecting interactions among TBN molecules and between TBN and Ag(111) that alter the dissociation dynamics of electronically excited TBN so as to produce more nascent NO in $v'' = 0$ than is found in the gas phase. While vibrational relaxation of nascent NO by collisions with the surface or neighboring species cannot be precluded, rotation and translation are typically relaxed more readily than vibration. REMPI state-resolved measurements of NO ejected from TBN on MgF_2 found no vibrational relaxation of the desorbed NO.[26]

Coverage Dependence. The variations with TBN coverage of the rotational and translational state distributions of the ejected NO during 351 nm photodissociation follow those reported for 248 nm photodissociation.[36] The relative contribution of the thermalized component increases linearly up to 5 ML as the fraction of NO formed and trapped beneath the adsorbate−vacuum interface increases. No significant amount of collisionless NO is found in the submonolayer photodissociation. The NO produced in the first layer may have its translational energy altered by interactions with Ag(111). Alternatively, alignment of TBN in the first layer may place the internal O−N bond away from the surface normal, out of range of our perpendicularly positioned ion detector. With increasing coverage, a more random alignment of TBN would increase the probability that the breaking O−N bond will be oriented along the surface normal. Consequently, the collisionless component would appear from the second and thicker layers. This hypothesis, supported by angle-resolved NO time-of-flight quadrupole mass analyzer

measurements without REMPI detection,[34] will be investigated in detail after we upgrade our detection system with angle-resolved REMPI capabilities. Surface roughness and 3D island formation[28−31] can account for the collisionless component growing for doses that exceed 2 ML of "effective coverage".

5. Summary

The 351 nm photodissociation of *tert*-butyl nitrite, adsorbed on Ag(111), has been studied by measuring the translational and internal state distributions of the photofragment NO using resonance enhanced multiphoton ionization time-of-flight (REMPI-TOF). Trimodal velocity distributions of the desorbed NO are observed and interpreted according to a collisional relaxation model proposed in our previous studies. The collisionless component originates from the topmost layer of the adsorbate, and nascent NO loses no energy in its exit trajectory. The slowest NO is due to full thermalization by the substrate and neighboring surface species. The intermediate NO suffers a few collisions and gives up part of its energy.

For the collisionless component, Gaussian distributions with $J_{max} = 24.5 \pm 1$ and $J_{max} = 29.5 \pm 1$ describe the rotational distributions of NO in $v'' = 1$ and 2. The lower J_{max} for $v'' = 1$ is the reverse of that observed in monomer gas-phase photolysis and is ascribed to alteration of the ground and/or excited-state potential energy surfaces of isolated TBN by interactions with neighboring species. A Boltzmann rotational state distribution, $T_{rot} = 124 \pm 30$ K, prevails for $v'' = 0$.

The relative vibrational populations for $v'' = 0$, 1, and 2 are 0.17, 0.41, and 0.42, respectively. While collisional relaxation may contribute, the high population at $v'' = 0$, compared to gas phase photolysis, is attributed mainly to the strong interactions among TBN molecules and between TBN and the silver substrate. These alter the excited-state potential energy surface and the vibrational distribution. The surface coverage has no effect on translational energies but does affect the relative intensities, reflecting changes in average adsorbate orientation and the composition of the local environment.

Acknowledgment. Support by the National Science Foundation, Grant No. CHE0070122, and by the Robert A. Welch Foundation is gratefully acknowledged. S.K.K. is supported by the Korea Science and Engineering Foundation (Grant 98-0591-01-01-3).

References and Notes

(1) Zhou, X.-L.; Zhu, X.-Y.; White, J. M. *Surf. Sci. Rep*. **1991**, *13*, 73.
(2) Dai, H.-L.; Ho, W., Ed. *Laser Spectroscopy and Photochemistry on Metal Surfaces*; Advances in Physical Chemistry Series; World Scientific: Singapore, 1995.
(3) Zimmermann, F. M.; Ho, W. *Surf. Sci. Rep.* **1995**, *22*, 127.
(4) Hodgson, A. *Prog. Surf. Sci*. **2000**, *63*, 1.
(5) Chuang, T. J. *Surf. Sci. Rep*. **1983**, *3*, 1.
(6) Ehrlich, D. J., Higashi, G. S., Oprysko, M. M., Eds. *Laser and Particle-Beam Chemical Processing for Microelectronics*; MRS Symposium Proceedings Vol. 101; Materials Research Society: Pittsburgh, PA, 1988.
(7) Calvert, J. G.; Pitts, J. M. *Photochemistry*; Wiley: New York, 1966.
(8) Schwartz-Lavi, D.; Bar, I.; Rosenwaks, S. R. *Chem. Phys. Lett.* **1986**, *128*, 123.
(9) Noble, N.; Qian, C. X. W.; Reisler, H.; Wittig, C. J. *Chem. Phys.* **1986**, *85*, 5763.
(10) Keller, S. A.; Felder, P.; Huber, J. R. *J. Phys. Chem.* **1987**, *91*, 1114.
(11) Lavi, R.; Schwartz-Lavi, D.; Bar, I.; Rosenwaks, S. *J. Phys. Chem.* **1987**, *91*, 5398
(12) August, J.; Brouard, M.; Docker, M. P.; Miline, C. J.; Simons, J. P.; Lavi, R.; Rosenwaks, S.; Schwartz-Lavi, D *J. Phys. Chem.* **1988**, *92*, 5485.
(13) Schwartz-Lavi, D.; Rosenwaks, S. *J. Chem. Phys.* **1998**, *88*, 6922.
(14) Winniczek, J. W.; Dubs, R. L.; Appling, J. R.; McKoy, V.; White, M. G. *J. Chem. Phys.* **1989**, *90*, 949.
(15) Effenhauser, C. S.; Felder, P.; Huber, J. R. *J. Phys. Chem.* **1990**, *94*, 296.
(16) Suter, H. U.; Brühlmann, U.; Huber, J. R. *Chem. Phys. Lett.* **1990**, *171*, 63.
(17) Hippler, M.; Al-Janabi, F. A. H.; Pfab, J. *Chem. Phys. Lett*. **1992**, *192*, 173.
(18) Hippler, M.; McCoustra, M. R. S.; Pfab, J. *Chem. Phys. Lett*. **1992**, *198*, 168.
(19) Kades, E.; Rösslein, M.; Huber, J. R. *Chem. Phys. Lett.* **1993**, *209*, 275.
(20) Mestdagh, J. M.; Berdah, M.; Dimicoli, I.; Mons, M.; Meynadier, P.; d'Oliveira, P.; Piuzzi, F.; Visticot, J. P.; Lardeux-Dedonder, C.; Martrenchard-Barra, S.; Soep, B.; Solgadi, D. *J. Chem. Phys.* **1995**, *103*, 1013.
(21) Rösslein, M.; Kades, E.; Bergmann, K.; Huber, J. R. *Chem. Phys. Lett.* **1995**, *235*, 242.
(22) Kades, E.; Rösslein, M.; Brühlmann, U.; Huber, J. R. *J. Phys. Chem.* **1993**, *97*, 989.
(23) Kades, E.; Rösslein, M.; Brühlmann, U.; Huber, J. R. *J. Phys. Chem.* **1994**, *98*, 13556.
(24) Bergmann, K.; Huber, J. R. *J. Phys. Chem. A* **1997**, *101*, 259.
(25) Simpson, C. J. M. S.; Griffiths, P. T.; Towrie, M. *Chem. Phys. Lett*. **1995**, *234*, 203.
(26) Simpson, C. J. M. S.; Griffiths, P. T.; Wallaart, H. L.; Towrie, M. *Chem. Phys. Lett.* **1996**, *263*, 19.
(27) Griffiths, P. T.; Simpson, C. J. M. S.; Stolte, C.; Towrie, M. *Chem. Phys. Lett.* **1999**, *315*, 158.
(28) Jenniskens, H. G.; van Essenberg, W.; Kadodwala, M.; Kleyn, A. W. *Chem. Phys. Lett.* **1997**, *268*, 7.
(29) Jenniskens, H. G.; van Essenberg, W.; Kadodwala, M.; Kleyn, A. W. *Surf. Sci.* **1998**, *402−404*, 140.
(30) Jenniskens, H. G.; Philippe, L.; van Essenberg, W.; Kadodwala, M.; Kleyn, A. W. *J. Chem. Phys.* **1988**, *108*, 1688.
(31) Jenniskens, H. G.; Philippe, L.; van Essenberg, W.; Kadodwala, M.; Kleyn, A. W. *J. Phys. Chem. B* **1988**, *102*, 8736.
(32) Pressley, L. A.; Pylant, E. D.; White, J. M. *Surf. Sci.* **1996**, *367*, 1.
(33) Fieberg, J. E.; Szulczewski, G. J.; White, J. M. *Chem. Phys. Lett.* **1998**, *290*, 268.
(34) Fieberg, J. E.; White, J. M. *Chem. Phys. Lett.* **1999**, *306*, 103.
(35) Kim, C.; Zhao, W.; White, J. M. *Surf. Sci.* **2000**, *464*, 240.
(36) Zhao, W.; Kim, C.; White, J. M. *Surf. Sci.* **2000**, *451*, 267.
(37) Furlan, A. *Chem. Phys. Lett.* **2000**, *321*, 339.
(38) Bray, R. G.; Hochstrasser, R. M.; Wessel, J. E. *Chem. Phys. Lett.* **1974**, *27*, 167.
(39) Bray, R. G.; Hochstrasser, R. M. *Mol. Phys.* **1976**, *31*, 1199.
(40) Engleman, R., Jr.; Rouse, P. E. *J. Mol. Spectrosc.* **1971**, *37*, 240.
(41) Gross, K. P.; McKenzie, R. L. *J. Chem. Phys.* **1982**, *76*, 5260.
(42) Mallard, W. G.; Miller, J. H.; Smyth, K. C. *J. Chem. Phys*. **1982**, *76*, 3483.
(43) Jacobs, D. C.; Zare, R. N. *J. Chem. Phys.* **1986**, *85*, 5457.
(44) Jacobs, D. C.; Madix, R. J.; Zare, R. N. *J. Chem. Phys.* **1985**, *85*, 5469.
(45) Schinke, R. *Photodissociation Dynamics*; Cambridge University Press: Cambridge, U.K., 1993.
(46) Giorgi, J. B.; Kühnemuth, R.; Polanyi, J. C. *J. Chem. Phys.* **2000**, *113*, 807.